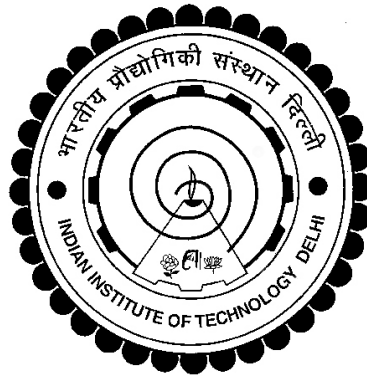


ANALYSIS, DESIGN AND CONTROL OF DC-DC CONVERTERS FOR GENERAL LIGHTING SYSTEMS

SOMNATH PAL



**DEPARTMENT OF ELECTRICAL ENGINEERING
INDIAN INSTITUTE OF TECHNOLOGY DELHI
DECEMBER 2020**

© Indian Institute of Technology Delhi (IITD), New Delhi, 2020

ANALYSIS, DESIGN AND CONTROL OF DC-DC CONVERTERS FOR GENERAL LIGHTING SYSTEMS

by

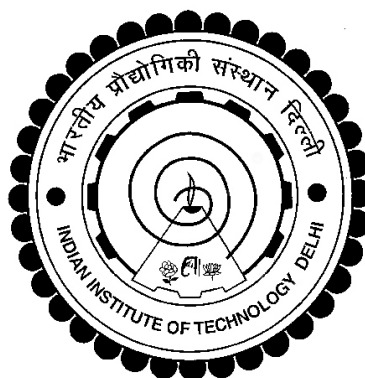
SOMNATH PAL

Department of Electrical Engineering

Submitted

in fulfillment of the requirements of the degree of DOCTOR OF PHILOSOPHY

to the



INDIAN INSTITUTE OF TECHNOLOGY DELHI

DECEMBER 2020

CERTIFICATE

This is certified that the thesis entitled, “**Analysis, Design and Control of DC-DC Converters for General Lighting Systems,**” being submitted by **Mr. Somnath Pal** for the award of the degree of **Doctor of Philosophy** is a record of the bonafide research work carried out by him in the Department of Electrical Engineering of Indian Institute of Technology Delhi.

Mr. Somnath Pal has fulfilled the requirements of this thesis work under my guidance and supervision, which to my knowledge has reached the requisite standard. The matters embodied in this thesis, have not been submitted to any other University or Institute for the award of any degree.

Dated:

(Prof. Bhim Singh)

Electrical Engineering Department
Indian Institute of Technology Delhi
Hauz Khas, New Delhi-110016, India

ACKNOWLEDGEMENTS

I would like to express my sincere gratitude and indebtedness to **Prof. Bhim Singh** for providing me an opportunity to carry out the Ph.D. work under his supervision. Working under him has been a wonderful experience, which has provided me with a deep insight into the world of research. From time to time, he encouraged me to excel in my work and it is his quest for excellence that has inspired me to improve my work and constantly introspect myself. His valuable suggestions, constant encouragement, and continuous monitoring have propelled me to complete the research with quality. I would like to thank him very much for his support and inspiration during my study and research.

My sincere thanks and deep gratitude are to my SRC members **Prof. S. Mishra, Prof. N. Senroy, and Dr. A. Verma**, for their encouragement, insightful comments, and hard questions that helped me a lot in my progress and presentations.

I take this opportunity to sincerely acknowledge the Indian Institute of Technology Delhi for providing excellent research facilities. Thanks are due to **Mr. Gurucharan Singh, Mr. Negi, Mr. Srichand, and Mr. Puran Singh**, laboratory staff of Power Electronics and PG Machines for their sustained help, exemplary attitude, and dedication to carry out my dissertation work.

I express my warm thanks to all of my friends and well-wishers Prof. Ashish Srivastava, Mr. Anshul Varshney, Dr. Nishant Kumar, and Dr. Aniket Anand. My thanks are also due to Mr. Praveen K Singh, Mr. Bodhibrata Mukhopadhyay, and Ms. Dedeepya Pappireddy who have given me immense moral support and co-operation to perform my work comfortably.

I must thank my colleagues at Philips India Limited (presently Signify Innovations India Limited), Noida during my tenure in this esteemed organization. My deepest sense of

gratitude to Mr. Amit Jain, Director Philips India Ltd. for his precious guidance that keeps me on the correct path and allowing me to carry out my research work. I would also like to express my special thanks to Mr. Shyam Singh for taking part in useful decisions and arranged all facilities to make life easier. I choose this moment to acknowledge his contribution much gratefully.

Words cannot express the feelings and gratitude I have for my **parents** for the constant unconditional encouragement, support, and personal sacrifices they made to push me forward to reach new levels of excellence. Finally, I thank my wife, Ms. Moumita Pal, for her inspiration, love that endorsed me to complete my research work. Her faith and belief in my capabilities have always encouraged me to achieve higher academic credentials. This dissertation stands as a testament to her unconditional adore and encouragement. Once again, I bow to all those who directly or indirectly helped me but their names are left out.

Somnath Pal.

Date: 30 Dec. 2020

Somnath Pal

Place: New Delhi

2014EEZ8316

ABSTRACT

Lighting (or illumination) characterizes the way an area is known to the human eye through either natural or artificial light. Natural light emanates predominantly from the sun. The intensity of sunlight varies in accordance with the time of day and the location. Buildings and premises are often designed to improve the capture of natural daylight. Alternatively, artificial light is human-made and can emerge from sources including fire, gaslight, candlelight, electric lamps, and so forth. At present, however, the term 'artificial lighting' essentially refers to lighting that comes from electric lamps. Artificial light as a rule is simply manipulated to achieve the required lighting result. The light can be enhanced or reduced, directed, focused, and colored. This enables lighting to produce a range of effects conferring to the requirements of a space. The term 'general lighting' relates to the background levels of light in a specific area. In the majority of workplaces, the optimal level of general lighting is determined in accordance with the best practices to ensure human safety and empower everyday visual tasks to be carried out comfortably and efficiently. General lighting may be foreseen merely by artificial lighting or a combination of artificial and natural light. The type of artificial light source adapted is to be determined by the type of space such as indoor or outdoor, and the lighting levels along with the quality and the energy consumption of the lighting luminaire. In recent years, it has been noticed an immense shift away from traditional incandescent filament light bulbs to more energy-savings alternatives. The exploration of new light sources such as the light-emitting diode (LED) has been made revolutionary changes in lighting design. Owing to its exclusive advantages, LED is replacing conventional light sources at a more rapid pace. When combined with advanced control gear, a clean, energy-efficient, and cost-effective lighting solution can be made for general lighting arrangements.

The LED driving technologies are primarily classified based on the required power demand. These are further classified on the basis of isolated or non-isolated outputs from the input AC mains. The conventional LED driving system comprises of DC-DC converters, which involves inferior control mechanism and excess component count that gives rise to unsatisfactory performances concerning power quality consideration and efficiency. In addition to this, the majority of converters are designed to operate within a short range of universal AC mains. The converter stability is quite unexplored and does not fulfill the constant voltage or constant current operation of the LED load. A large ripple in the LED drive current is often witnessed, which leads to unwanted flicker in the light produced. Moreover, due to increasing uses of artificial light sources, lighting also accountable for

significant energy consumption over the past few years. As a consequence, several studies are conducted on energy-saving lighting solutions, which are reported in the literature.

In this research work, the analysis, design, control, and development of several DC-DC converters are carried out with the view of improving the aforementioned drawbacks. The DC-DC converters, which are explored as LED drivers are aimed at four fundamental aspects, namely the power quality improvement over a wide operational range, increasing converter efficiency, development of cost-effective dimming concepts, and reducing design complexity with improved stability. The research work is also focused on various lighting demands starting from very low power for household applications to high power industrial uses. In each stage, appropriate DC-DC converters are studied and developed in line with the foregoing aspects that give rise to satisfactory performances over the conventional topologies used in LED lighting systems. The trouble with poor efficiency in isolated converters, is further improved and eradicated the limitations of low power applications for single-stage converters. This research work has also explored the conventional single-stage DC-DC converters in high power lighting demands by shifting the operating trends from discontinuous conduction mode (DCM) to critical conduction mode (CrCM). Taking advantage of CrCM operation and proper controller design, improved power quality performances, and efficiency are achieved in the proposed DC-DC converters. Moreover, in high power LED loads, the need for improved power quality parameters and efficiency are more important along with the precise regulations. In order to satisfy the above criteria, two-stage converter solutions are implemented where the first-stage is responsible for the power factor correction (PFC) over universal AC mains, and the second-stage precisely controls the load regulation with isolation. In terms of converter stability during transient and dynamic operations, a comprehensive study of stability performances using the state-space analysis model for all the DC-DC converters, is carried out and implemented in hardware prototypes.

This research work also investigates on low-cost energy-savings dimming concepts, which are integrated into the DC-DC converters and completely retrofitted. The primary drawback of excessive harmonic contents in AC mains current during dimming operations in the conventional low-cost dimming practices, is addressed and improved power quality performances are made available through the proposed dimming concepts. Furthermore, all the converter topologies and dimming models are presented in this research work, are using minimal circuit components, reliable in operation, and applicable for upcoming LED lighting solutions.

सारांश

प्रकाश व्यवस्था (या रोशनी) उस तरह की विशेषता है जैसे कि किसी क्षेत्र को प्राकृतिक या कृत्रिम प्रकाश के माध्यम से मानव आंखों के लिए जाना जाता है। प्राकृतिक प्रकाश मुख्य रूप से सूर्य से निकलता है। सूर्य के प्रकाश की तीव्रता दिन के समय और स्थान के अनुसार बदलती रहती है। इमारतों और परिसर अक्सर प्राकृतिक दिन के उजाले को प्राप्त करने के लिए डिज़ाइन किए जाते हैं। वैकल्पिक रूप से, कृत्रिम प्रकाश मानव निर्मित है और आग, गैसलाइट, मोमबत्ती की रोशनी, बिजली के लैंप, और अन्य स्रोतों से उभर सकता है। वर्तमान में, हालांकि, 'कृत्रिम प्रकाश व्यवस्था' शब्द अनिवार्य रूप से प्रकाश व्यवस्था को संदर्भित करता है जो बिजली के लैंप से आता है। एक नियम के रूप में कृत्रिम प्रकाश को आवश्यक प्रकाश परिणाम प्राप्त करने के लिए बस सफाई से उपयोग किया जाता है। प्रकाश को बढ़ाया या कम किया जा सकता है, निर्देशित किया जा सकता है, केंद्रित किया जा सकता है, और रंगीन बनाया जा सकता है। यह प्रकाश को जगह की आवश्यकताओं के अनुरूप प्रभाव की एक श्रृंखला का उत्पादन करने में सक्षम बनाता है। 'सामान्य सामान्य प्रकाश व्यवस्था' शब्द एक विशिष्ट क्षेत्र में प्रकाश की पृष्ठभूमि के स्तर से संबंधित है। अधिकांश कार्यस्थलों में, सामान्य प्रकाश व्यवस्था का इष्टतम स्तर मानव सुरक्षा सुनिश्चित करने और रोजमर्रा के दृश्य कार्यों को आराम से और कुशलता से संपन्न करने के लिए सर्वोत्तम प्रथाओं के अनुसार निर्धारित किया जाता है। सामान्य प्रकाश व्यवस्था केवल कृत्रिम प्रकाश व्यवस्था या कृत्रिम और प्राकृतिक प्रकाश के संयोजन से ही हो सकती है। अनुकूलित किए गए कृत्रिम प्रकाश स्रोत को जगह के प्रकार जैसे कि घर के अंदर या बाहर, और प्रकाश स्तर के साथ-साथ गुणवत्ता और प्रकाश लुमिनेर की ऊर्जा खपत द्वारा निर्धारित किया जाता है। हाल के वर्षों में, यह देखा गया है कि पारंपरिक तापदीप्त प्रकाश बल्बों की जगह ऊर्जा-बचत बिकल्प एक बड़ा बदलाव है। प्रकाश उत्सर्जक डायोड (एलईडी) जैसे नए प्रकाश स्रोतों की खोज में प्रकाश व्यवस्था के डिज़ाइन में क्रांतिकारी बदलाव किए गए हैं। अपने विशेष लाभों के कारण, एलईडी पारंपरिक प्रकाश स्रोतों को अधिक तीव्र गति से बदल रहा है। उन्नत नियंत्रण गियर के साथ संयुक्त होने पर, सामान्य प्रकाश व्यवस्था के लिए एक स्वच्छ, ऊर्जा-कुशल और लागत प्रभावी प्रकाश समाधान किया जा सकता है।

एलईडी ड्राइविंग प्रौद्योगिकियों को मुख्य रूप से आवश्यक बिजली की मांग के आधार पर वर्गीकृत किया जाता है। इन्हें इनपुट एसी मेन से पृथक या गैर-पृथक आउटपुट के आधार पर आगे वर्गीकृत किया गया है। पारंपरिक एलईडी ड्राइविंग सिस्टम में डीसी-डीसी कन्वर्टर शामिल हैं, जिसमें अवर नियंत्रण तंत्र और अतिरिक्त घटक गणना शामिल है जो बिजली की गुणवत्ता पर विचार और दक्षता से संबंधित असंतोषजनक प्रदर्शनों को जन्म देती है। इसके अतिरिक्त, अधिकांश कन्वर्टर को यूनिवर्सल एसी मेन की एक छोटी सीमा के भीतर संचालित करने के लिए डिज़ाइन किया गया है। कनवर्टर स्थिरता काफी अस्पष्ट है और एलईडी लोड के निरंतर वोल्टेज या निरंतर करंट संचालन को पूरा नहीं करता है। एलईडी ड्राइव करंट में एक

बड़ी रिप्ल अक्सर देखी जाती है, जिससे उत्पादित प्रकाश में अवांछित झिलमिलाहट होती है। इसके अलावा, कृत्रिम प्रकाश स्रोतों के बढ़ते उपयोग के कारण, पिछले कुछ वर्षों में महत्वपूर्ण ऊर्जा खपत के लिए प्रकाश व्यवस्था भी जिम्मेदार है। परिणामस्वरूप, ऊर्जा-बचत प्रकाश समाधानों पर कई अध्ययन किए जाते हैं, जो साहित्य में रिपोर्ट किए गए हैं।

इस शोध कार्य में, कई डीसी-डीसी कन्वर्टर के विश्लेषण, डिजाइन, नियंत्रण और विकास को उपरोक्त कमियों को सुधारने के दृष्टिकोण से किया गया है। डीसी-डीसी कन्वर्टर, जिन्हें एलईडी ड्राइवों के रूप में खोजा गया है, का उद्देश्य चार मूलभूत पहलुओं, अर्थात् एक व्यापक परिचालन सीमा पर बिजली की गुणवत्ता में सुधार, कनवर्टर दक्षता में वृद्धि, लागत प्रभावी डिमिंग अवधारणाओं का विकास और बेहतर स्थिरता के साथ डिजाइन जटिलता को कम करना है। अनुसंधान कार्य विभिन्न प्रकाश मांगों पर भी ध्यान केंद्रित किया गया है जो घरेलू अनुप्रयोगों के लिए उच्च शक्ति औद्योगिक उपयोगों के लिए बहुत कम बिजली से शुरू होता है। प्रत्येक चरण में, उपयुक्त डीसी-डीसी कन्वर्टर का अध्ययन किया गया है और पूर्वगामी पहलुओं के अनुरूप विकसित किया गया है जो एलईडी प्रकाश व्यवस्था में उपयोग किए जाने वाले पारंपरिक टोपोलॉजी पर संतोषजनक प्रदर्शन को जन्म देता है। आइसोलेटेड कन्वर्टर में खराब दक्षता के साथ परेशानी, एकल चरण के कन्वर्टर के लिए कम बिजली अनुप्रयोगों की सीमाओं को और बेहतर बनाया गया है। इस शोध कार्य में पारंपरिक सिंगल-स्टेज डीसी-डीसी कन्वर्टर को हाई पावर लाइटिंग डिमांड्स में डिस्कन्टीन्यूस कंडक्शन मोड को क्रिटिकल कंडक्शन मोड में परिवर्तित करके उपयोग किया गया है। प्रस्तावित डीसी-डीसी कन्वर्टर में सीआरसीएम संचालन और उचित नियंत्रक डिजाइन का लाभ उठाते हुए, बेहतर बिजली की गुणवत्ता और दक्षता को प्राप्त किया गया है। इसके अलावा, उच्च शक्ति वाले एलईडी लोड में, सटीक नियमों के साथ-साथ बेहतर बिजली गुणवत्ता मापदंडों और दक्षता की आवश्यकता अधिक महत्वपूर्ण है। उपरोक्त मानदंडों को पूरा करने के लिए, दो-चरण कनवर्टर समाधान कार्यान्वित किए जाते हैं, जहां पहला चरण यूनिवर्सल एसी मेन पर पावर फैक्टर करेक्शन (पीएफसी) के लिए जिम्मेदार होता है, और दूसरा चरण अलगाव के साथ लोड विनियमन को नियंत्रित करता है। क्षणिक और गतिशील संचालन के दौरान कनवर्टर स्थिरता के संदर्भ में, सभी डीसी-डीसी कन्वर्टर के लिए स्टेट-स्पेस विश्लेषण मॉडल का उपयोग करके स्थिरता प्रदर्शन का एक व्यापक अध्ययन किया गया है और हार्डवेयर प्रोटोटाइप में कार्यान्वित किया गया है।

यह शोध कार्य कम-लागत वाली ऊर्जा-बचत डिमिंग अवधारणाओं पर भी जांच करता है, जिन्हें डीसी-डीसी कन्वर्टर में एकीकृत किया गया है और पूरी तरह से रेट्रोफिट किया गया है। पारंपरिक कम लागत वाली डिमिंग प्रथाओं में मद्धिम संचालन के दौरान एसी मेन करंट में अत्यधिक हार्मोनिक कंटेंट की प्राथमिक खामी को संबोधित किया गया है और प्रस्तावित डिमिंग अवधारणाओं के माध्यम से बेहतर गुणवत्ता वाले प्रदर्शन उपलब्ध कराए गए हैं। इसके अलावा, सभी कनवर्टर टोपोलॉजी और डिमिंग मॉडल इस शोध कार्य में प्रस्तुत किए गए हैं, जो न्यूनतम सर्किट घटकों का उपयोग कर रहे हैं, संचालन में विश्वसनीय हैं, और आगामी एलईडी लाइटिंग समाधानों के लिए लागू हैं।

TABLE OF CONTENTS

	Page No.
Certificate	i
Acknowledgments	ii
Abstract (English)	iv
Abstract (Hindi)	vi
Table of Contents	viii
List of Figures	xv
List of Tables	xxiii
List of Abbreviations	xxiv
List of Symbols	xxvii
CHAPTER I INTRODUCTION	1-16
1.1 General	1
1.2 Classifications of Artificial Light Sources	2
1.2.1 Incandescent	2
1.2.2 Halogen	2
1.2.3 Fluorescent	2
1.2.4 High-Intensity Discharge (HID) Lamps	3
1.2.5 Light-Emitting Diode (LED)	3
1.3 Classifications of LEDs in General Illumination Systems	5
1.4 Power Quality and Safety Concerns in LED Lighting	7
1.4.1 Power Quality Parameters in LED Lighting	8
1.4.2 Power Quality Standards	9
1.4.3 Safety Standards	10
1.5 Objectives of Proposed Work	11
1.5.1 Analysis, Design, Modeling, and Development of Single-Stage Isolated and Non-Isolated PFC DC-DC Converters in LED Driving Systems	11
1.5.2 Analysis, Design, Modeling, and Development of Two-Stage DC-DC PFC Converter fed Isolated Resonant Converters in LED Driving Systems	12
1.5.3 Analysis, Design, Modeling, and Development of Low-Cost Retrofit Dimming Concepts in Lighting Design	12

1.6	Outline of Chapters	12
CHAPTER II LITERATURE REVIEW		17-38
2.1	General	17
2.2	Overview of DC-DC Converters in LED Lighting	18
2.3	Review of Different Approaches for Power Quality Improvement in LED Lighting Systems	19
2.3.1	Passive PFC Approach	19
2.3.2	Active PFC Approach	20
2.4	State of Art of Various Topologies Explored in LED Lighting Systems	21
2.4.1	Review of Single-Stage, Non-Isolated DC-DC PFC Converters in LED Lighting Systems	22
2.4.2	Review of Single-Stage, Isolated DC-DC PFC Converters in LED Lighting Systems	27
2.4.3	Review of Two-Stage, Non-Isolated Converters in LED Lighting Arrangements	30
2.4.4	Review of Two-Stage, Isolated Converters in LED Lighting Practices	31
2.5	Review of Energy-Saving Dimming Technologies in LED Lighting Architectures	33
2.5.1	Analog Dimming Approaches	33
2.5.2	PWM Dimming Approaches	34
2.5.3	Programmable Dimming Approaches	35
2.6	Identified Research Areas	36
2.7	Conclusions	37
CHAPTER III ANALYSIS, DESIGN, MODELING, AND DEVELOPMENT OF A UNIVERSAL INPUT NON-ISOLATED LUO PFC CONVERTER WITH PILOT-LINE DIMMING CONCEPT IN LED LIGHTING SYSTEMS		39-68
3.1	General	39
3.2	Configuration of Non-Isolated Luo Converter based LED Driver	40
3.3	Working Principle of PFC Luo Converter in CrCM	41
3.4	Design of Luo Converter using LED Load over Universal AC Mains Operations	44
3.4.1	Duty Ratio Calculation	44
3.4.2	Design of Input Inductor	45
3.4.3	Design of Intermediate Capacitor	46
3.4.4	Design of Output Inductor	46

3.4.5	Design of DC-Link Capacitor	47
3.4.6	Design of Input Side Filter Capacitor	47
3.5	Stability Analysis of Luo Converter using Small Signal Analysis	48
3.5.1	Control Algorithm of Luo Converter in Open-Loop System	48
3.5.2	Control Algorithm of Luo Converter in Closed-Loop System	52
3.6	Pilot-Line Dimming Concept Integrated with Luo Converter	54
3.6.1	Generation of Sinusoidal AC Mains Current	55
3.6.2	Operating Principle of Pilot-Line Dimming Concept	55
3.7	Results and Discussion	59
3.7.1	Experimental Validation of Non-Isolated Luo Converter as a PFC	59
3.7.2	Validation of CrCM and Constant Current Operations over Universal AC Mains	61
3.7.3	A Dimming Example and PQ Performances	62
3.7.4	Experimental Electrical Performances under Full Load and Dimming Operations	65
3.8	Conclusions	68
CHAPTER IV	ANALYSIS, DESIGN, MODELING, AND DEVELOPMENT OF A WIDE-INPUT-EXTREME-OUTPUT (WIEO) TAPPED-INDUCTOR BUCK-BOOST CONVERTER FOR EFFICIENCY IMPROVEMENT IN LED LIGHTING ARRANGEMENTS	69-96
4.1	General	69
4.2	Configurations of Diode-Tapped and Switch-Tapped Versions of Buck-Boost Converter	70
4.3	Design of Diode-Tapped and Switch-Tapped Buck-Boost Converters in CrCM	71
4.3.1	Design of Critical Inductances	74
4.3.2	Design of DC-link Capacitors	74
4.4	Small-Signal State-Space Modeling of Tapped-Inductor Buck-Boost Converters	75
4.4.1	Stability Analysis of Diode-Tapped Buck-Boost Converter	76
4.4.2	Stability Analysis of Switch-Tapped Buck-Boost Converter	80
4.5	Results and Discussion	84
4.5.1	PFC Performances and Load Regulations over Universal AC Mains	85
4.5.2	Validation of CrCM Operation	89
4.5.3	Switching Stress Analysis and Improvement of Converter Efficiency	90

4.5.4	Dimming Performances	92
4.5.5	Experimental Electrical Parameters	93
4.6	Conclusions	95
CHAPTER V	DESIGN, SIMULATION, AND IMPLEMENTATION OF A UNIVERSAL INPUT PFC CSC (CANONICAL SWITCHING CELL) CONVERTER IN LOW POWER LED LIGHTING SYSTEMS	97-116
5.1	General	97
5.2	Configuration and Working Principle of Non-Isolated CSC Converter in DICM	98
5.3	Design Procedure of CSC Converter over Universal AC Mains	101
5.3.1	Design of Input Inductor	101
5.3.2	Design of Intermediate Capacitor	102
5.3.3	Design of DC-link Capacitor	102
5.3.4	Design of Filter Capacitor	103
5.4	Control of DICM CSC Converter	104
5.5	Results and Discussion	105
5.5.1	Simulated Performance of PFC CSC Converter	105
5.5.2	Experimental Validation of CSC Converter as a Constant Current LED Driver	108
5.5.2.1	Validation of CSC Converter as a PFC	108
5.5.2.2	Validation of Constant Current Operation	110
5.5.2.3	Validation of DICM Operation and Efficiency Improvement	111
5.5.2.4	Experimental Electrical Performance Parameters for Full Load and Half Load Conditions	113
5.6	Conclusions	115
CHAPTER VI	ANALYSIS, DESIGN, MODELING, AND DEVELOPMENT OF A CRCM FLYBACK CONVERTER IN HIGH POWER LED LIGHTING APPLICATIONS	117-140
6.1	General	117
6.2	Working Principle of Flyback Converter in CrCM	118
6.3	Design of PFC Flyback Converter under Universal AC Mains Operation	120
6.3.1	Design of Primary Inductance	123
6.3.2	Design of Turns Ratio of Transformer	124
6.3.3	Design of Output DC-Link Capacitor	124
6.3.4	Selection of Semiconductor Components	124

6.3.5	Design of Snubber Elements	125
6.4	Study of Stability Performances using State-Space Analysis	126
6.4.1	Stability Analysis under Open-Loop Condition	126
6.4.2	Stability Analysis under Closed-Loop Condition	128
6.5	Wide-Output Operation using External VCC Supply	130
6.6	Results and Discussion	131
6.6.1	Validation of PFC Performances	132
6.6.2	Validation of Constant Voltage Operation and Stability Performances	134
6.6.3	Ripple Reduction using 2 nd Stage LC Filter	135
6.6.4	CrCM Operation and Stresses on Semiconductor Components	136
6.6.5	Experimental Electrical Parameters and Power Loss Analysis	138
6.7	Conclusions	139
CHAPTER VII	ANALYSIS, DESIGN, MODELING, AND DEVELOPMENT OF AN ISOLATED SINGLE-ENDED PRIMARY INDUCTANCE CONVERTER BASED LED DRIVER WITH DISTORTIONLESS DIMMING ARRANGEMENTS	141-165
7.1	General	141
7.2	Working Principle of Isolated SEPIC Converter in CrCM	142
7.3	Design Consideration under Universal AC Mains	145
7.3.1	Design of Critical Inductances	146
7.3.2	Design of AC Coupling Capacitor	146
7.3.3	Design of Output DC-link Capacitor	147
7.3.4	Design of Line Filter Capacitor	147
7.4	Stability Analysis of CrCM SEPIC in Isolated Configuration	148
7.4.1	Stability Analysis in Open-Loop Control	148
7.4.2	Stability Analysis in Closed-Loop Control	151
7.5	Operating Principle of Distortionless Dimming Concept Integrated into Isolated SEPIC Control Gear	152
7.6	Results and Discussion	157
7.6.1	Experimental Validation of Isolated SEPIC as a PFC with Nonlinear LED Load under Full Output Operation	158
7.6.2	Validation of Power Quality Performances in Dimming Operation	160
7.6.3	Validation of Converter Stability	161
7.6.4	Experimental Electrical Parameters and Efficiency Improvement	162
7.7	Conclusions	165

CHAPTER VIII ANALYSIS, DESIGN, MODELING, AND DEVELOPMENT OF A TWO-STAGE ZETA PFC FED LLC RESONANT CONVERTER IN HIGH BRIGHTNESS LED LIGHTING DESIGN 166-192

8.1	General	166
8.2	Principle of Operation of First-Stage PFC Zeta Converter in CrCM	167
8.3	Working Principle of Second-Stage LLC Resonant Converter	169
8.4	Design of PFC Zeta Converter in CrCM	172
8.4.1	Specifications of Input and Output Parameters of PFC Stage	172
8.4.2	Design of Input and Output Inductances	173
8.4.3	Design of Energy Transfer Capacitor	174
8.4.4	Design of DC-bus Capacitor	174
8.5	Design of Second-Stage LLC Resonant converter	174
8.5.1	Specifications of Input and Output Parameters of LLC Resonant Stage	175
8.5.2	Gain Characteristics of LLC Resonant Cell	175
8.5.3	Design of Transformer Turns Ratio	177
8.5.4	Design of Equivalent Load Resistance	177
8.5.5	Design of Voltage Gain	177
8.5.6	Design of Resonant Circuit Parameters	177
8.6	Stability Analysis for Constant DC-bus Operation using SSA	178
8.6.1	Stability under Open-Loop Condition	181
8.6.2	Stability Improvement under Closed-Loop Condition	182
8.7	Results and Discussion	184
8.7.1	Validation of PFC Performances	185
8.7.2	Validation of Constant DC-Bus Operation and Bus Voltage Stability	187
8.7.3	Validation of Constant Current Operation	188
8.7.4	Validation of ZVS Operation and Efficiency Improvement	189
8.7.5	Experimental Electrical Parameters	190
8.8	Conclusions	191

CHAPTER IX ANALYSIS, DESIGN, MODELING, AND DEVELOPMENT OF A UNIVERSAL INPUT BOOST PFC FED LLC RESONANT CONVERTER IN HIGH POWER LED LIGHTING SYSTEMS 193-216

9.1	General	193
9.2	Configuration of PFC Boost Converter Fed LLC Resonant Converter	194

9.3	Design of CrCM Boost Converter	195
9.3.1	Design of Input Filter Capacitor	195
9.3.2	Design of DC-Bus Capacitor	196
9.3.3	Design of Boost Converter Inductor	196
9.4	Design of Second-Stage LLC Resonant Cell	197
9.4.1	Design of Turns Ratio and Reflected Load Resistance	197
9.4.2	Design of Minimum and Maximum Gains	198
9.4.3	Design of LLC Resonant Cell	198
9.4.4	Design of Resonance and Switching Frequencies	200
9.5	CrCM Operation of PFC Boost Converter	200
9.6	Stability Analysis using SSA for Boost Converter	202
9.6.1	Stability under Open-Loop Control	204
9.6.2	Stability under Closed-Loop Control	205
9.7	Results and Discussion	207
9.7.1	Validation of PFC Performances	208
9.7.2	Validation of CV Operation and Bus Voltage Stability	211
9.7.3	Validation of ZVS Operation and Converter Efficiency	212
9.7.4	Experimental Electrical Performances under Full Load and Half load Operations	214
9.8	Conclusions	215
CHAPTER X	MAIN CONCLUSIONS AND SUGGESTIONS FOR FURTHER WORK	217-224
10.1	General	217
10.2	Fundamental Contributions, Comparisons, and Limitations	218
10.3	Main Conclusions	219
10.4	Suggestions for Further Work	223
	REFERENCES	225-247
	APPENDICES	248-255
	LIST OF PUBLICATIONS	256-256
	BIO-DATA	257-257

LIST OF FIGURES

- Fig. 3.1 Non-isolated Luo converter in source grounded configuration.
- Fig. 3.2 Operation of PFC Luo converter in CrCM. (a) Mode I, (b) Mode II, (c) Waveforms.
- Fig. 3.3 Bode plots of Luo converter (a) Open-loop systems, (b) Closed-loop systems.
- Fig. 3.4 Type-II Compensation network of Luo converter in a closed-loop system.
- Fig. 3.5 Hardware prototype of proposed pilot-line dimming concept using a non-isolated Luo converter.
- Fig. 3.6 Sinusoidal AC input current generation in a PFC Luo converter.
- Fig. 3.7 Voltage across CP_1 , CP_2 and A , B w.r.t. GND in the dimming circuit of Luo converter (Scale: Horizontal: 20 ms/div, Vertical: 200 V/div).
- Fig. 3.8 Voltage across R_2 , R_4 and C_4 w.r.t. GND in the dimming circuit of Luo converter (Scale: Horizontal: 100 ms/div, Vertical: 10 V/div).
- Fig. 3.9 Clamping of V_{cs} during dimming and sinusoidal AC mains current generation in a Luo converter.
- Fig. 3.10 Waveforms of PFC Luo converter for source voltage $v_s(t)$, and source current $i_s(t)$. Scale (Horizontal: 10ms/div, Vertical: $v_s(t)$: 200 V/div; $i_s(t)$: 400 mA/div; at AC mains voltage operation of 85 V.
- Fig. 3.11 Waveforms of PFC Luo converter for source voltage $v_s(t)$, and source current $i_s(t)$. Scale (Horizontal: 10ms/div, Vertical: $v_s(t)$: 200 V/div; $i_s(t)$: 250 mA/div; at AC mains voltage operation of 265 V.
- Fig. 3.12 PF attained in hardware prototype of PFC Luo converter for Full load and 30% Dimming Load over universal AC mains.
- Fig. 3.13 THDi obtained from hardware prototype of PFC Luo converter for Full load and 30% Dimming Load over universal AC mains.
- Fig. 3.14 Waveforms of output DC voltage V_{dc} , and output DC current I_{dc} for Luo converter. Scale (Horizontal: 5 ms/div, Vertical: V_{dc} : 17 V/div I_{dc} : 200 mA/div) for the AC mains voltage of 85 V.
- Fig. 3.15 Waveforms of output DC voltage V_{dc} , and output DC current I_{dc} . for Luo converter. Scale (Horizontal: 5 ms/div, Vertical: V_{dc} : 17 V/div I_{dc} : 200 mA/div) for the AC mains voltage of 265 V.
- Fig. 3.16 Waveforms of Luo converter for drain-source voltage $V_{DS(S1)}$ and drain current $I_{D(S1)}$ of switching MOSFET, S_1 . Scale (Horizontal: 10 μ s/div, Vertical: $V_{DS(S1)}$: 200 V/div; $I_{D(S1)}$: 300 mA/div for nominal AC mains voltage of 230 V.
- Fig. 3.17 Voltage and current waveforms of Luo converter for switching diode D_1 . Scale (Horizontal: 10 μ s/div, Vertical: $V_{a(D1)}$: 100 V/div; $I_{a(D1)}$: 700 mA/div for nominal AC mains voltage of 230 V.
- Fig. 3.18 Various circuit parameter waveforms of Luo converter before and after dimming. Scale (Horizontal: 20 ms/div, Vertical: $v_s(t)$: 240 V/div; $i_s(t)$, I_{dc} : 500 mA/div; V_{dc} : 50 V/div) for AC mains operation of 230 V.

- Fig. 3.19 Various circuit parameter waveforms of Luo converter before and after dimming. Scale (Horizontal: 20 ms/div, Vertical: $v_s(t)$: 240 V/div; $i_s(t)$, I_{dc} : 500 mA/div; V_{dc} : 50 V/div) for AC mains operation of 115 V.
- Fig. 3.20 Various circuit parameter waveforms of Luo converter at 30% dimming condition. Scale (Horizontal: 20 ms/div, Vertical: $v_s(t)$: 240 V/div; $i_s(t)$, I_{dc} : 500 mA/div; V_{dc} : 50 V/div) for AC mains operation of 230 V.
- Fig. 3.21 Efficiency vs. source voltage plot of Luo converter at full load and 30% dimming load.
- Fig. 3.22 Harmonic contents in AC mains current of PFC Luo converter at 265 V mains operation and associated limits as per IEC 61000-3-2.
- Fig. 3.23 Photograph of the hardware prototype of non-isolated Luo converter based LED driver.
- Fig. 4.1 Diode-tapped buck-boost converter in a step-down configuration.
- Fig. 4.2 Switch-tapped buck-boost converter in a step-up configuration.
- Fig. 4.3 Transfer characteristics of diode-tapped buck-boost converter.
- Fig. 4.4 Transfer characteristics of switch-tapped buck-boost converter.
- Fig. 4.5 Open-loop Bode Plot of diode-tapped buck-boost converter with a PM of 2.93° and GM of infinity.
- Fig. 4.6 Closed-loop Bode Plot of diode-tapped buck-boost converter with a GM of 37 dB and PM of 90° .
- Fig. 4.7 Type-II compensation network for closed-loop control of the diode-tapped buck-boost converter.
- Fig. 4.8 Open-loop Bode Plot of switch-tapped buck-boost converter with a PM of 3.41° and GM of infinity.
- Fig. 4.9 Closed-loop Bode Plot of switch-tapped buck-boost converter with PM of 90.2° and GM of 25.2 dB.
- Fig. 4.10 Type-II compensation network for closed-loop control of switch-tapped buck-boost converter.
- Fig. 4.11 Schematic of hardware prototype for diode-tapped version of the buck-boost converter.
- Fig. 4.12 Experimental waveforms of input voltage $v_{s1}(t)$, $\{scale:120 V/div\}$; input current $i_{s1}(t)$, $\{scale:0.8 A/div\}$ output DC voltage V_{dc1} , $\{scale:3.5 V/div\}$ and output DC current I_{dc1} , $\{scale:1.5 A/div\}$ for 85 V AC mains of the diode-tapped step-down circuit. *Time scale:10 ms/div.*
- Fig. 4.13 Experimental waveforms of input voltage $v_{s1}(t)$, $\{scale:120 V/div\}$; input current $i_{s1}(t)$, $\{scale:0.5 A/div\}$ output DC voltage V_{dc1} , $\{scale:3.5 V/div\}$ and output DC current I_{dc1} , $\{scale:1.5 A/div\}$ for 265 V AC mains of the diode-tapped step-down circuit. *Time scale:10 ms/div.*
- Fig. 4.14 Experimental waveforms of input voltage $v_{s2}(t)$, $\{scale:120 V/div\}$; input current $i_{s2}(t)$, $\{scale:0.8 A/div\}$ output DC voltage V_{dc2} , $\{scale:100 V/div\}$ and output DC current I_{dc2} , $\{scale:50 mA/div\}$ for 85 V AC mains of the switch-tapped step-up circuit. *Time scale:10 ms/div.*

- Fig. 4.15 Experimental waveforms of input voltage $v_{s2}(t)$, $\{scale:120 V/div\}$; input current $i_{s2}(t)$, $\{scale:0.5 A/div\}$ output DC voltage V_{dc2} , $\{scale:100 V/div\}$ and output DC current I_{dc2} , $\{scale:50 mA/div\}$ for 265 V AC mains of the switch-tapped step-up circuit. *Time scale:10 ms/div.*
- Fig. 4.16 PF and THDi variations over universal AC mains for diode-tapped buck-boost converter.
- Fig. 4.17 PF and THDi variations over universal AC mains for switch-tapped buck-boost converter.
- Fig. 4.18 Harmonic spectrum of diode-tapped and switch-tapped versions at 265 V AC mains.
- Fig. 4.19 Waveforms of currents through the inductors L_1 for diode-tapped, $\{scale:1.5 A/div\}$ and L_2 for switch-tapped converters $\{scale:0.15A/div\}$; at 230 V AC mains. *Time scale:5 μ s/div.*
- Fig. 4.20 Waveforms of switch voltage (Yellow) and switch current (Red) for diode-tapped (S_1), $\{scale:100V/div, 0.5A/div\}$ and switch-tapped (S_2), $\{scale:150V/div, 0.15A/div\}$; at 230V AC mains. *Time scale:5 μ s/div.*
- Fig. 4.21 Efficiency comparison between diode-tapped and untapped versions of the buck-boost converter in step-down operation.
- Fig. 4.22 Efficiency comparison between switch-tapped and untapped versions of the buck-boost converter in step-up operation.
- Fig. 4.23 Thermal imaging analysis of the diode-tapped converter for loss distribution.
- Fig. 4.24 PF and THDi performances during 30% dimming operation of diode-tapped circuit
- Fig. 4.25 PF and THDi performances during 30% dimming operation of switch-tapped circuit.
- Fig. 5.1 Configuration of non-isolated CSC converter with inverting LED load.
- Fig. 5.2 Modes of operations of CSC converter in DICM and associated waveforms. (a) Mode I, (b) Mode II, (c) Waveforms.
- Fig. 5.3 PFC Control of DICM CSC converter.
- Fig. 5.4 Voltage and current waveforms of different circuit elements in CSC converter at 85 V AC mains operations.
- Fig. 5.5 Voltage and current waveforms of different circuit elements in CSC converter at 230 V AC mains operations.
- Fig. 5.6 Voltage and current waveforms of different circuit elements in CSC converter at 265 V AC mains operations.
- Fig. 5.7 Simulated waveforms of AC mains current and harmonic spectrum in CSC converter. (a) 85 V AC mains operation, (b) 230 V AC mains operation, (c) 265 V AC mains operation.
- Fig. 5.8 Photograph of hardware prototype for CSC converter based LED driver.
- Fig. 5.9 Experimental waveforms of CSC converter for input current at 85 V AC mains operation (Scale, Vert: 100 V/div, 250 mA/div; Horizontal: 10 ms/div).

- Fig. 5.10 Experimental waveforms of CSC converter for input current at 230 V AC mains operation (Scale, Vert: 100 V/div, 160 mA/div; Horizontal: 10 ms/div).
- Fig. 5.11 Experimental waveforms of CSC converter for input current at 265 V AC mains operation (Scale, Vert: 100 V/div, 140 mA/div; Horizontal: 10 ms/div).
- Fig. 5.12 PF variation of PFC CSC converter over universal AC mains.
- Fig. 5.13 THDi variation of PFC CSC converter over universal AC mains.
- Fig. 5.14 Harmonic Spectrum of PFC CSC converter at 265 V AC mains operation.
- Fig. 5.15 Voltage and current waveforms of CSC converter for the LED load at 85 V AC mains operation (Scale, Vert: 10 V/div, 210 mA/div; Horizontal: 10 ms/div).
- Fig. 5.16 Voltage and current waveforms of CSC converter for the LED load at 230 V AC mains operation (Scale, Vert: 10 V/div, 210 mA/div; Horizontal: 10 ms/div).
- Fig. 5.17 Voltage and current waveforms of CSC converter for the LED load at 265 V AC mains operation (Scale, Vert: 10 V/div, 210 mA/div; Horizontal: 10 ms/div).
- Fig. 5.18 Experimental waveshape of CSC converter for the voltage across the intermediate capacitor at 265 V AC mains operation (Scale, Vertical: 140 V/div; Horizontal: 10 ms/div).
- Fig. 5.19 Experimental waveforms of switching stresses recorded at 85 V AC mains condition in CSC converter (Scale, Vertical: 50 V/div, 1 A/div; Horizontal: 10 ms/div, for zoomed waveshapes, Vertical: 65 V/div, 1 A/div; Horizontal: 5 μ s/div).
- Fig. 5.20 Efficiency variation of CSC converter over universal AC mains.
- Fig. 6.1 Configuration of flyback converter with 2nd stage LC filter and multi-string LED load.
- Fig. 6.2 Working principle of flyback converter in CrCM operation. (a) Mode I, (b) Mode II, (c) Waveforms
- Fig. 6.3 Waveforms of sinusoidal current generation over a half cycle in a PFC flyback converter.
- Fig. 6.4 Open-loop Bode plot of flyback converter in CrCM operation.
- Fig. 6.5 Closed-loop Bode plot of flyback converter in CrCM operation.
- Fig. 6.6 Hardware prototype schematic of flyback converter consisting of 2nd stage LC filter, and Type-II compensator blocks.
- Fig. 6.7 Supply voltage $v_s(t)$ and supply current $i_s(t)$ waveforms of flyback converter at AC mains operation of 85 V. Scale (Horizontal: 10 ms/div; Vertical: $v_s(t)$: 100 V/div; $i_s(t)$: 500 mA/div.).
- Fig. 6.8 Supply voltage $v_s(t)$ and supply current $i_s(t)$ waveforms of flyback converter at AC mains operation of 265 V. Scale (Horizontal: 10 ms/div; Vertical: $v_s(t)$: 100 V/div; $i_s(t)$: 320 mA/div.).
- Fig. 6.9 PF variation of the CrCM flyback converter for full load and half load operations.
- Fig. 6.10 THDi characteristics of PFC flyback converter over universal AC mains for full load and half load operations.

- Fig. 6.11 Harmonic spectrum of PFC flyback converter at 265 V AC mains operation for full load and half load conditions.
- Fig. 6.12 Waveforms of output DC voltage V_{dc} and output DC current I_{dc} of CrCM flyback converter at AC mains operation of 85 V. Scale (Horizontal: 10 ms/div; Vertical: V_{dc} : 15 V/div; I_{dc} : 550 mA/div).
- Fig. 6.13 Waveforms of output DC voltage V_{dc} and output DC current I_{dc} of CrCM flyback converter at AC mains operation of 265 V. Scale (Horizontal: 10 ms/div; Vertical: V_{dc} : 15 V/div; I_{dc} : 550 mA/div).
- Fig. 6.14 Waveform of output voltage stability during the transition of the input voltage from 85 V to 265 V in CrCM flyback converter. Scale (Horizontal: 50 ms/div.).
- Fig. 6.15 Waveforms of output voltage ripple without 2nd stage LC filter in flyback converter at AC supply voltage of 265 V. Scale (Horizontal: 10 ms/div; Vertical: V_{dc} : 5 V/div.).
- Fig. 6.16 Waveforms of output voltage ripple with 2nd stage LC filter in flyback converter at AC supply voltage of 265 V. Scale (Horizontal: 10 ms/div; Vertical: V_{dc} : 5 V/div.).
- Fig. 6.17 Primary inductor current of CrCM flyback converter at AC supply voltage of 85 V. Scale (Horizontal: Un-zoomed (5 ms/div), Zoomed (8.5 μ s/div); Vertical: 1.5 A/div.).
- Fig. 6.18 Waveforms of CrCM flyback converter for drain current and drain-source voltage of the switching MOSFET, S_1 at AC supply voltage of 85 V. Scale (Horizontal: 6.5 μ s/div; Vertical: $V_{DS(S1)}$: 60 V/div; $I_{D(S1)}$: 2 A/div.).
- Fig. 6.19 Waveforms of CrCM flyback converter for drain current and drain-source voltage of the switching MOSFET, S_1 at an AC supply voltage of 265 V. Scale (Horizontal: 7 μ s/div; Vertical: $V_{DS(S1)}$: 100 V/div; $I_{D(S1)}$: 1.5 A/div.).
- Fig. 6.20 Waveforms of CrCM flyback converter captured for current and voltage stresses of switching diode D_1 at AC mains voltage of 265 V. Scale (Horizontal: 6 μ s/div; Vertical: $V_{d(D1)}$: 250 V/div; $I_{d(D1)}$: 5 A/div.).
- Fig. 6.21 Efficiency comparison of the proposed converter in CrCM and traditional flyback converter in DCM.
- Fig. 7.1 Isolated SEPIC control gear with LED lighting load.
- Fig. 7.2 Current through various circuit components of isolated SEPIC in CrCM operation. (a) Mode I, (b) Mode II (c) Waveforms.
- Fig. 7.3 Operation of CrCM SEPIC with primary-side sensing.
- Fig. 7.4 Open-loop Bode plot of CrCM SEPIC.
- Fig. 7.5 Closed-loop Bode plot of CrCM SEPIC.
- Fig. 7.6 Schematic of hardware prototype with different blocks responsible for the operation of SEPIC.
- Fig. 7.7 Waveforms of isolated SEPIC for different circuit parameters before and after dimming (Scale: Vertical: 150 V/div for $v_s(t)$, 1.5 V/div for CK , Gates of M_1 & M_2 , and 250 mA/div for I_{dc} . Horizontal: 500 ms/div.) (a) 50% dimming example (b) 10% dimming example.

- Fig. 7.8 Developed hardware prototype of isolated SEPIC.
- Fig. 7.9 Experimental setup for development of isolated SEPIC with LED load.
- Fig. 7.10 Waveforms of input AC mains voltage and mains current at 85 V AC mains operation in a PFC SEPIC. (Scale: Ver. 125 V/div.; 400 mA/div.; Hor. 10 ms/div.).
- Fig. 7.11 Waveforms of input AC mains voltage and mains current at 265 V AC mains operation in a PFC SEPIC. (Scale: Ver. 125 V/div.; 250 mA/div.; Hor. 10 ms/div.).
- Fig. 7.12 PF variations of PFC SEPIC under universal AC mains operations for full load and 50% dimming load.
- Fig. 7.13 THDi variations of PFC DEPIC under universal AC mains operations for full load and 50% dimming load.
- Fig. 7.14 Waveforms of input AC mains voltage and mains current in a PFC SEPIC at 265 V AC mains operation during 50% dimming operation. (Scale: Ver. 120 V/div.; 185 mA/div.; Hor. 10 ms/div.).
- Fig. 7.15 Harmonic spectrum of isolated SEPIC as per IEC 61000-3-2 at 265 V AC mains operation.
- Fig. 7.16 Output LED load voltage and load current of isolated SEPIC during full load operation. (Scale: Vertical: 20 V/div, 500 mA/div. Horizontal: 10 ms/div.).
- Fig. 7.17 Waveforms of start-up stability in isolated SEPIC. (Scale: Vertical: 250 V/div for $v_s(t)$, 30 V/div for V_{dc} and 500 mA/div for I_{dc} . Horizontal: 500 ms/div).
- Fig. 7.18 Efficiency comparison between isolated SEPIC and flyback converter.
- Fig. 8.1 Configuration of non-isolated Zeta converter.
- Fig. 8.2 Modes of operation of PFC Zeta converter in source grounded configuration. (a) Mode I, (b) Mode II.
- Fig. 8.3 Operational modes of half-bridge LLC resonant converter for $f_{s(HB)} > f_r$. (a) Mode I, (b) Mode II, (c) Mode III, (d) Mode IV.
- Fig. 8.4 Operating waveforms of LLC resonant converter above the resonance frequency.
- Fig. 8.5 Equivalent circuit of LLC resonant converter. (a) Non-linear non-sinusoidal circuit, (b) Linear sinusoidal circuit.
- Fig. 8.6 Gain vs frequency characteristics of LLC resonant cell.
- Fig. 8.7 Open-loop Bode plot of CrCM Zeta converter.
- Fig. 8.8 Closed-loop Bode plot of CrCM Zeta converter.
- Fig. 8.9 Schematic of Zeta PFC fed LLC resonant converter for an experimental prototype.
- Fig. 8.10 Waveforms of the input voltage $v_s(t)$ and input current $i_s(t)$ for input AC voltage operation of 85 V in a two-stage Zeta PFC fed LLC converter. (Scale: Vertical 225V/div, 1.4 A/div; Horizontal 10 ms/div.).

- Fig. 8.11 Waveforms of input voltage $v_s(t)$ and input current $i_s(t)$ for input AC voltage operation of 265V in a two-stage Zeta PFC fed LLC converter.(Scale: Vertical 225 V/div, 1.4 A/div; Horizontal 10 ms/div.).
- Fig. 8.12 PF and THDi variations of two-stage Zeta-LLC converter under universal AC mains operations.
- Fig. 8.13 Harmonic spectrum of two-stage Zeta-LLC converter at 265 V AC mains operation.
- Fig. 8.14 Waveforms of input voltage $v_s(t)$, and DC-bus voltage V_{bus} for input AC voltage operation of 85 V in a Zeta-LLC converter. (Scale: Vertical 200 V/div for $v_s(t)$, 100 V/div for V_{bus} ; Horizontal 10 ms/div.).
- Fig. 8.15 Waveforms of input voltage $v_s(t)$, and DC-bus voltage V_{bus} for input AC voltage operation of 265 V in a Zeta-LLC converter. (Scale: Vertical 220 V/div for $v_s(t)$, 100 V/div for V_{bus} ; Horizontal 10 ms/div.).
- Fig. 8.16 Waveforms of input voltage $v_s(t)$, and DC-bus voltage V_{bus} for the bus voltage stability in a Zeta-LLC converter. (Scale: Vertical 245 V/div for $v_s(t)$, 135 V/div for V_{bus} ; Horizontal 200 ms/div.).
- Fig. 8.17 Waveforms of output voltage, V_{dc} and output current, I_{dc} for input AC voltage, $v_s(t)$ operation of 85 V in a Zeta-LLC converter. (Scale: Vertical 225 V/div for $v_s(t)$, 25 V/div for V_{dc} and 2 A/div for I_{dc} ; Horizontal 10 ms/div.).
- Fig. 8.18 Waveforms of output voltage, V_{dc} and output current, I_{dc} for input AC voltage, $v_s(t)$ operation of 265 V in a Zeta-LLC converter. (Scale: Vertical 225 V/div for $v_s(t)$, 25 V/div for V_{dc} and 2 A/div for I_{dc} ; Horizontal 10 ms/div.).
- Fig. 8.19 Drain to source voltage and current waveforms of half-bridge switching MOSFET S_3 for input AC voltage operation of 230 V in a Zeta-LLC converter. (Scale: Vertical 135 V/div, 500 mA/div.; Horizontal 10 ms/div, Zoomed: 9.5 μ s/div.)
- Fig. 8.20 Efficiency comparisons between the proposed two-stage Zeta-LLC converter and the conventional converters over universal AC mains operations.
- Fig. 8.21 Experimental hardware prototype of a two-stage Zeta-LLC converter.
- Fig. 9.1 Circuit configuration of two-stage boost PFC fed LLC resonant converter with multi-string LED load.
- Fig. 9.2 Voltage gain plot of the LLC resonant network for $L_k = 4$.
- Fig. 9.3 Controller for PFC operation of a boost converter with Type-II compensator.
- Fig. 9.4 Open-loop Bode plot of CrCM boost converter.
- Fig. 9.5 Closed-loop Bode plot of CrCM boost converter.
- Fig. 9.6 Schematic for hardware prototype of a two-stage boost PFC fed LLC resonant converter.
- Fig. 9.7 Full load input current waveform under input AC voltage operation of 85 V in a boost-LLC converter. (Scale: Ver. $v_s(t)$: 230 V/div., $i_s(t)$: 2 A/div. Hor. 10 ms/div.).

- Fig. 9.8 Full load input current waveform under input AC voltage operation of 265 V in a boost-LLC converter. (Scale: Ver. $v_s(t)$: 230 V/div., $i_s(t)$: 1.6 A/div. Hor. 10 ms/div.).
- Fig. 9.9 PF variations in a two-stage boost-LLC converter over universal AC mains operations.
- Fig. 9.10 THDi performances in a two-stage boost-LLC converter over universal AC mains operations.
- Fig. 9.11 Spectrum of AC mains current harmonics at 265 V operation in a boost-LLC converter.
- Fig. 9.12 Waveforms of output LED voltage and LED current at 85 V AC mains operation in a boost-LLC converter. (Scale: Ver. V_{dc} : 35 V/div., I_{dc} : 900 mA/div. Hor. 10 ms/div.).
- Fig. 9.13 Waveforms of bus voltage stability during a transition of 85 V to 265 V in a boost-LLC converter. (Scale: Ver. $v_s(t)$: 245 V/div., V_{bus} : 135 V/div. Hor. 200 ms/div.).
- Fig. 9.14 Waveforms of bus voltage stability during a transition of 265 V to 85 V in a boost-LLC converter. (Scale: Ver. $v_s(t)$: 245 V/div., V_{bus} : 135 V/div. Hor. 200 ms/div.).
- Fig. 9.15 Full load switching waveforms of boost MOSFET, S_1 at 85 V AC mains operation. (Scale: Ver. $V_{DS(S1)}$: 120 V/div., $I_{D(S1)}$: 2.2 A/div. Hor. 5 ms/div., for Zoomed: 15 μ s/div.).
- Fig. 9.16 Full load switching waveforms of HB switching MOSFET, S_3 at 265 V AC mains operation. (Scale: Ver. V_{HB} : 120 V/div., $I_{D(S3)}$: 530 mA/div. Hor. 7.5 μ s/div.).
- Fig. 9.17 Efficiency variations of two-stage boost-LLC converter over universal AC mains operations.

LIST OF TABLES

Table 3.1	Summary of Calculated and Selected Circuit Parameters for Non-Isolated Luo Converter
Table 3.2	Power Conditions at Different Switching Position of Pilot-Line Dimming Operation
Table 3.3	Electrical Performance Parameters of Luo Converter during Full Load Operation
Table 3.4	Electrical Performance Parameters of Luo Converter at 30% Dimming Load Operation
Table 4.1	Summary of Designed Circuit Parameters for Diode-Tapped and Switch-Tapped Buck-Boost Converters
Table 4.2	Electrical Performance Parameters of Diode-Tapped Buck-Boost Converter in a Step-Down Operation
Table 4.3	Electrical Performance Parameters of Switch-Tapped Buck-Boost Converter in a Step-Up Operation
Table 5.1	Comparisons of Single-Stage, Single-Switch Non-Isolated DC-DC Converters
Table 5.2	Summary of Calculated and Selected Design Parameters for CSC Converter
Table 5.3	Power Loss Distributions in Different Circuit Elements of CSC Converter
Table 5.4	Full Load Electrical Performance Parameters of CSC Converter
Table 5.5	Half Load Electrical Performance Parameters of CSC Converter
Table 6.1	Summary of Calculated and Selected Values for Flyback Converter
Table 6.2	Electrical Performance Parameters Recorded from the Hardware Prototype of Flyback Converter
Table 6.3	Power Loss Calculations in Different Circuit Components of Flyback Converter
Table 7.1	Summary of Calculated and Selected Design Parameters for Isolated SEPIC
Table 7.2	Bill of Materials for Experimental Prototype of Isolated SEPIC
Table 7.3	Comparison between SEPIC and Flyback Converters
Table 7.4	Electrical Performance Parameters during Full Load Operation of Isolated SEPIC
Table 7.5	Electrical Performance Parameters at 50% Dimming Operation of Isolated SEPIC
Table 8.1	Summary of Calculated and Selected Design Parameters of Two-Stage Zeta-LLC Converter
Table 8.2	Experimental Performance Parameters of Zeta PFC fed LLC Resonant Converter
Table 9.1	Summary of Calculated and Selected Design Parameters of Two-Stage Boost-LLC Converter
Table 9.2	Full Load Performance Parameters of Boost PFC fed LLC Resonant Converter
Table 9.3	Half Load Performance Parameters of Boost PFC fed LLC Resonant Converter
Table 10.1	Outcomes of all the Proposed Converters in General Lighting Applications

LIST OF ABBREVIATIONS

AC	Alternating Current
AM	Amplitude Modulation
BW	Bandwidth
CCM	Continuous Conduction Mode
CCW	Counter Clockwise
CFL	Compact Fluorescent Lamp
CK	Clock
CS	Current Sense
CSC	Canonical Switching Cell
CrCM	Critical Conduction Mode
DALI	Digital Addressable Lighting Interface
DBR	Diode Bridge Rectifier
DC	Direct Current
DCM	Discontinuous Conduction Mode
DCVM	Discontinuous Capacitor Voltage Mode
DICM	Discontinuous Inductor Current Mode
DPF	Displacement Power Factor
DT	Diode-Tapped
EMI	Electro-Magnetic Interference
GaN	Gallium Nitride
GM	Gain Margin
GND	Ground
HB	Half-Bridge
HBLED	High-Brightness LED

HID	High-Intensity Discharge
HISLLC	Hybrid Input Super Lift Luo Converter
IC	Integrated Circuits
IoT	Internet of Things
LED	Light-Emitting Diode
MOSFET	Metal–Oxide–Semiconductor Field-Effect Transistor
op-amp	Operational Amplifiers
PCB	Printed Circuit Board
PCC	Point of Common Coupling
PF	Power Factor
PFC	Power Factor Correction
PI	Proportional–Integral
PM	Phase Margin
POESL	Positive Output Elementary Super Lift
PQ	Power Quality
PQI	Power Quality Improvement
PSR	Primary-Side Regulation
PWM	Pulse-Width Modulation
QR	Quasi-Resonant
RMS	Root Mean Square
SEPIC	Single-Ended Primary Inductance Converter
Si	Silicon
SIMO	Single-Inductor Multiple-Outputs
SMPS	Switched-Mode Power Supply
SSA	State-Space Analysis
SSR	Secondary-Side Regulation

ST	Switch-Tapped
TRIAC	Triode For Alternating Current
THDi	Total Harmonic Distortion of the input current
UV	Ultraviolet
UVLO	Under-Voltage Lockout
VCC	Voltage Common Collector, the power input of a device
WIEO	Wide Input and Extreme Output
ZCS	Zero-Current Switching
ZCD	Zero-Crossing Detection
ZVS	Zero-Voltage Switching

LIST OF SYMBOLS

C_f	Filter capacitor after the bridge rectifier
C_l	Intermediate coupling capacitor
C_{dc}	Output DC capacitor across LED load
$C(s)$	Controller transfer function
C_{bus}	DC bus capacitor
d_1, d_2	Duty ratios
D	Diode
f_l	AC line frequency
f_s	Switching frequency of DC-DC PFC converter
$G_{vd}(s)$	Control-to-output transfer function
$G_o(s)$	Open-loop gain
$G_c(s)$	Closed-loop gain
$G_{dc}(s)$	Transfer function of the pulse width generator
$H(s)$	Scaling factor
$i_s(t)$	Supply AC input current
$I_{in}(t)$	Rectified input AC current
$I_{in(pk)}$	Peak input current of the AC mains
i_{L1}, i_{L2}	Current through the inductors L_1 and L_2
$\Delta i_{L1}, \Delta i_{L2}$	Ripple current through the inductors L_1 and L_2
$i_{pri}(t)$	Primary current of the transformer
$i_{sec}(t)$	Secondary current of the transformer
$I_{pk(pri)}$	Peak primary current of the transformer
$I_{pk(sec)}$	Peak secondary current of the transformer
$I_{DS(S1)}$	Drain-source current through the MOSFET S_1

$I_{d(D1)}$	Current through the diode D_1
L_1, L_2	Inductors
L_{pri}	Primary inductance of the transformer
L_{sec}	Secondary inductance of the transformer
$L_{1(cri)}, L_{2(cri)}$	Critical inductances
L_{lk}	Leakage inductance
M_v, M_1, M_2	Voltage Gain
N	Turns ration of the transformer
n_{pri}	Number of primary turns of the transformer
n_{sec}	Number of secondary turns of the transformer
n_{aux}	Number of auxiliary turns of the transformer
P_{in}	Input power of the converter
P_{dc}	Output power of the converter
R_{dc}	DC equivalent resistance of the LED load
R_{cs}	Current sense resistor
$R_{DS(ON)}$	Drain-Source on-resistance of a MOSFET
r_b	Equivalent load resistance seen by the DC-bus
S_1, S_2, S_3	Power MOSFETs
SW_1, SW_2	Switches
T_s	Time period for a switching cycle of power MOSFET
Tr_1	Transformer
$v_s(t)$	Supply input AC voltage
$V_{in}(t)$	Rectified input AC voltage
$V_{in(pk)}$	Peak supply voltage of the AC mains
$V_{in(min)}$	Rectified minimum input AC voltage
$V_{in(max)}$	Rectified maximum input AC voltage

V_{dc}	DC voltage across the LED load
ΔV_{dc}	Ripple voltage over V_{dc}
V_{C1}	Voltage across the intermediate capacitor
ΔV_{C1}	Ripple voltage over V_{C1}
V_{ref}	Reference voltage
$V_{DS(S1)}$	Drain-source voltage of the MOSFET S_1
$V_{d(D1)}$	Voltage across diode D_1
V_F	Forward voltage of diodes
V_{CE}	Collector-emitter voltage of transistors
V_G	Gate voltage of MOSFETs
V_{bus}	DC bus voltage
V_{HB}	Square-wave voltage
ω_l	Angular line frequency of the AC input voltage
θ	Displacement angle between the supply AC voltage and AC current
ϕ	Magnetic flux